HHS Public Access

Author manuscript

Nat Methods. Author manuscript; available in PMC 2024 August 15.

Published in final edited form as:

Nat Methods. 2023 November ; 20(11): 1666–1671. doi:10.1038/s41592-023-02030-7.

Molecular Mechanocytometry Using Tension-activated Cell Tagging

Rong Ma[1], **Sk Aysha Rashid**[1,*], **Arventh Velusamy**[1,*], **Brendan R. Deal**[1,*], **Wenchun Chen**[2], **Brian Petrich**[2], **Renhao Li**[2], **Khalid Salaita**[1,3]

[1]Department of Chemistry, Emory University

[2]Department of Pediatrics, Emory University

[3]Wallace H. Coulter Department of Biomedical Engineering, Emory University and Georgia Institute of Technology

Abstract

Flow cytometry is routinely used to measure single-cell gene expression by staining cells with fluorescent antibodies and nucleic acids. Here we present Tension-activated Cell Tagging (TaCT) to fluorescently label cells based on the magnitude of molecular force transmitted through cell adhesion receptors. As a proof-of-concept, we analyzed fibroblasts and mouse platelets after TaCT using conventional flow cytometry.

Using antibodies and complementary nucleic acids to fluorescently label cells followed by analysis using flow cytometry and Fluorescence-activated Cell Sorting (FACS) is a cornerstone of modern biological sciences. It would be highly desirable to also measure the mechanical profile of single cells using flow cytometry as this offers a complementary *biophysical* marker to chemical markers.[1–3] Accordingly, a suite of flow cytometry methods have been developed to readout cell mechanics by measuring cell deformation during hydrodynamic stretching or micro-constriction.[4–6] For example, in real-time deformability cytometry, a high-speed camera records the transient deformation of cells while passing through a narrow channel under shear flow.[7] Deformation-based cytometry methods are powerful and have demonstrated clinical potential by detecting disease-specific changes in the mechanical deformation of cells.[8, 9] One challenge for deformability measurements is these are a convoluted product of multiple parameters that include cell volume, membrane composition, cytoskeletal dynamics, and cell cycle.[10–13] Thus, there is a need to develop mechanophenotyping platforms that employ molecular markers of

Corresponding author: k.salaita@emory.edu.

*These authors contributed equally to this work.

Author Contributions Statement

R.M. and K.S. conceived the idea and wrote the manuscript. R.M., A.V., A.R., and B.R.D. carried out experiments and data analysis. A.V. performed oxDNA simulation. W.C., R.L., and B.P. provide mouse platelets. All authors contributed to editing the manuscript.

Competing Interests Statement

The authors declare no competing interests.

Code availability statement

Code used for oxDNA data analysis and graph generation is publicly available online at https://github.com/SalaitaLab/Tension_activated_cell_tagging.

mechanotransduction. To date, the readout of molecular forces generated by cells is performed using high-resolution fluorescence microscopy, which is low throughput. Indeed, there are no flow cytometry or FACS-like techniques that can tag/sort cells based on the magnitude of molecular forces generated (Table S1).[14, 15]

To address this gap, we present Tension-activated Cell Tagging (TaCT) (Figure 1A), which enables flow cytometry-based identification and sorting of mechanically active cells based on the molecular forces transmitted by their surface adhesion receptors. TaCT probes are engineered DNA duplexes that have a digital response to pN force and release a cholesterol-modified strand that spontaneously incorporates into the membrane of force-generating cells.

TaCT takes advantage of the fundamental mechanism of double stranded DNA “peeling” under force.[16] When a short DNA duplex is stretched from both ends of one of the strands (Figure 1B, i. 3’–5’ pulling), the duplex is destabilized, and can denature (Figure 1B, ii. peeling), leading to complementary DNA separation (Figure 1B, iii. separation).[16–18] Due to the narrow range of forces at which the denaturation transition occurs (Figure 1B, Figure S1), it can be characterized as a simple two-state system, i.e., we can treat the DNA duplex as either being in dsDNA form or in completely separated ssDNA form. For example, a 24mer duplex (Table S2) was reported to peel at F=41 pN using magnetic tweezer measurements.[16] To confirm the critical peeling force for this 24mer, we used the oxDNA coarse-grained model to apply a load of 2.81×10^3 nm/s and recorded the number of base pairs in the duplex.[19] The peeling force (F_{peel}) was defined as the force at which the number of base pairs in the duplex is ≤5. We found that F_{peel}=41±2.8 pN (mean±SD) by averaging the first 100 data points in the simulation (Figure 1B, Video S1, Figure S1).

The TaCT probe was comprised of a load-bearing strand and a 24mer peeling strand. The load-bearing strand displayed the RGD integrin ligand at one terminus and was attached to the glass slide through its other terminus. The loading-bearing strand also incorporated an internal Cy3B dye. The complementary peeling strand was designed to release once $F>F_{peel}$ and its termini were labeled with Atto647N and cholesterol (Figure 1A, Figure S2). TaCT probes were annealed and immobilized on streptavidin-coated glass slides (Figure S3). At rest, the probe is duplexed and Cy3B and Atto647N form a FRET pair. When $F>F_{peel}$, the Atto647N strand peels and dissociates, while the Cy3B dye on the load-bearing strand is de-quenched. The FRET efficiency for TaCT probes was 93.8% and hence the Cy3B signal is enhanced by >10 fold upon peeling (Figure S4A). The probe density was measured at 5200±286 molecules/μm^2, which then allowed us to convert the Cy3B fluorescence signal to %peel (Figure S4B, C).[20, 21]

To demonstrate that cell-generated forces drive DNA duplex peeling, mouse embryonic fibroblasts (MEF) were plated on TaCT probe surfaces and then imaged using conventional fluorescence microscopy (Figure 1C, v2). A timelapse showed cell spreading that coincided with Cy3B signal, confirming integrin binding to RGD on TaCT probes. The Cy3B signal was primarily localized to the cell edge, consistent with the distribution of focal adhesions (FAs), and accumulated over time (Figure 1D). The growth of Cy3B signal corresponded to the loss of Atto647N signal, confirming force-induced peeling (Figure 1E). This mechanism

can generate high quality maps of integrin forces independent of cholesterol conjugation to the probe (Extended Figure 1A, Figure S5). Quantitative microscopy analysis of 227 cells showed that 0.9±0.3% of probes peeled under each cell, equivalent to ~47±16 mechanical events/μm^2 with F>41 pN (Extended Figure 1B). The observed tension signal colocalized with markers of FAs such as vinculin and phosphorylated focal adhesion kinase (FAK pY397), as well as actin stress fibers (Extended Figure 1C, D, E), confirming that forces were primarily transmitted by integrins within FAs.[22] Importantly, the peeling signal mirrors that of the turn-on tension gauge tether (TGT) probes (Extended Figure 2A, B) but avoids the termination of mechanotransduction, which represents a major advantage as a molecular force sensor (Extended Figure 2A, C, D, Supplementary Note). Control groups of cells treated with Latrunculin B (Lat B), which inhibits actin polymerization and disrupts force generation, showed significantly reduced peeling signal, as expected (Extended Figure 3A, B). Cells treated with Lat B 50 min after seeding did not show tension signal changes, validating that the peeling mechanism is irreversible producing maps of accumulated mechanical events over time. As expected, addition of soluble peeling strand led to the loss of the tension signal in cells treated with Lat B, showing a simple approach to resetting tension signal and recording real-time events (Extended Figure 3C, D, E, F).

After confirming that DNA peeling faithfully maps molecular traction forces, we next investigated cholesterol-DNA cell tagging for TaCT (Figure 1A). Prior work showed that cholesterol-DNA can partition into the plasma membrane of cells.[23, 24] We discovered that cholesterol-ssDNA conjugates are ~50 fold more effective at tagging cells compared to cholesterol-dsDNA conjugates (Extended Figure 4A, B, Figure S6). This is advantageous as it enhances the specificity of TaCT. We also verified that cholesterol-ssDNA membrane association is linearly proportional to the soluble conjugate concentrations tested (Extended Figure 4C, D).[24] The stability of TaCT tags was examined by incubating cholesterol-ssDNA with cells, washing, and measuring the loss of DNA as a function of time. We found that ~20–30% of the cholesterol-tethered DNA dissociated at 90 min (Extended Figure 4E, F). Accordingly, we chose to incubate the cells on the surface for 1 h, which allowed for focal adhesion formation and TaCT to proceed while limiting cholesterol dissociation.

As a proof-of-concept, NIH3T3 cells were seeded onto the TaCT substrates, allowed to spread and then collected by gentle scraping. TaCT signal was then measured by flow cytometry. Probes lacking RGD, probes lacking cholesterol as well as full TaCT probes but with cells treated with Lat B were used as negative controls. The resulting flow cytometry histograms showed a heterogeneous distribution of TaCT signal, matching the tension signal distributions observed under microscopy (Figure 1F, Extended Figure 1B). The cells on the TaCT substrate showed 27.6±4.0% force positive population compared to 0.6±0.2%, 1.1±0.5%, and 3.5±2.0% in (−)cholesterol, (−)RGD, and (+)Lat B controls, respectively (Figure 1F, Extended Figure 5). The Atto647N geometric mean fluorescence intensity (gMFI) of cells incubated on TaCT showed a >2-fold increase compared to controls, whereas the Cy3B gMFI did not change (Extended Figure 5). Taken together, this result confirmed that TaCT is triggered by force transmission through the integrin-RGD complex, followed by cholesterol-mediated membrane incorporation. Background tagging of cells due to cell spreading and proximity to the surface leads to negligible TaCT signal (Extended Figure 6).

Next, we tested whether this strategy works in primary cells. Platelets were chosen for this demonstration as mechanical forces play a crucial role in platelet activation, aggregation, and clot retraction, which are necessary steps in coagulation.[25] When mouse platelets were seeded onto the TaCT surface for 30 min, we noted loss of Atto647N signal that was coupled with an increase in Cy3B. This confirms that platelet integrin force transmission was sufficient to mediate DNA peeling with F>41 pN (Figure 1G). The Atto647N depletion signal did not colocalize exclusively with the Cy3B turn-on signal, which may be due to the accumulation of cholesterol-DNA probes at the basal face of the cell membrane (Extended Figure 7A, B). Nonetheless, the TaCT signal was measured by flow cytometry, which showed 13.3±2% force positive population (Figure 1H, Extended figure 7C). Control experiments withholding the divalent cations Mg^{2+} or Ca^{2+} necessary for full integrin activation showed minimal TaCT signal and force positive population. Likewise, withholding ADP agonist inhibited platelet forces generation and TaCT signal, consistent with literature precedent.[25, 26] Finally, withholding ADP but adding Mn^{2+} led to cell spreading but without platelet activation and this control also showed weak TaCT signal. Together, these experiments demonstrate that TaCT specifically tags platelets based on integrin molecular traction forces.

To showcase that TaCT is an effective method to report cell receptor forces, we used a Rho-associated protein kinase (ROCK) inhibitor, Y27632, to disrupt the force transmission through cytoskeleton and measure the dose-dependent response in MEF cells. Y27632 inhibits ROCK kinases by competing with ATP binding, and further results in decreased myosin activity, destabilization of actin filaments and abolished stress fiber formation (Figure 1I).[27] With Y27632 pre-treatment, MEF cells showed decreased Cy3B tension signal (Figure 1J, Figure S7). TaCT signal measured by flow cytometry showed a clear dose-dependent curve (Figure 1K) with an IC50= 773 nM, agreeing well with microscopy measurements and literature reported IC50 values from 100’s of nM to low μM.[28]

After demonstrating TaCT with a single population of cells, we sought to demonstrate analysis of a binary mixture of cells with differing mechanical activity. We used parental MEF cells (wildtype, WT) and MEF cells with vinculin null (vin-) for this demonstration. Vinculin is an adaptor protein that localizes to FAs linking the cytoskeleton to adhesion receptors and aids in FA maturation (Extended Figure 1A).[29] We first performed TaCT on these two cell types separately. The vin- cells were stained with cell tracker dye CMFDA before plating onto TaCT substrates (Figure 2A). To ensure that the TaCT signal is not due to differential uptake, cholesterol uptake of WT and vin- cells was measured by flow cytometry in parallel with each TaCT assay (Figure S8). As shown in Figure 2B and C, WT cells had larger spreading area and produced more tension signal compared to vin- cells in the Cy3B channel. Flow cytometry also showed that there was more Atto647N signal in WT compared to vin- (Figure 2D, Figure S8) (WT: 26.6±3.7%, vin- 4.5±0.3%). We then tested if this differential tension signal could be detected when the WT and vin- were co-cultured (Figure 2E). As expected, the WT cells displayed more TaCT tension signal by microscopy compared to vin- cells despite effectively spreading on the substrate (Figure 2F). The WT TaCT signal decreased slightly when these cells were co-cultured, with a 24.4±3.7% force positive population compared to 5.2±1.0% for vin- in the mixed population (Figure 2G). The minimal TaCT signal change observed for vin- cells in co-culture indicated

that TaCT tags remain associated with target cells within the experimental time window (Figure S8). Together, these results confirm that TaCT can distinguish mechanically active subpopulations in heterogeneous mixtures of cells. To further demonstrate that TaCT produces a gradual response rather than a binary signal, we transfected MEF vin- cells with different amount of plasmid encoding GFP-vinculin (Figure 2H). We next investigated the relationship between vinculin expression and tension by quantifying GFP and Atto647 intensity at the single cell level. As expected, both the GFP and TaCT signal increased with increasing amount of the plasmid (Figure S9). Interestingly, the TaCT signal recovered with relatively low levels of GFP-vinculin, showing a linear regime followed by saturation of tension at increasing levels of vinculin, which indicates a complex relationship between integrin tension and vinculin expression (Figure 2I).

In conclusion, we take advantage of 3'–5' mediated DNA peeling to develop a new class of DNA tension probes to map the molecular forces generated by cells and to enable high-throughput flow-cytometry based detection of mechanically active cells. As is the case for all DNA tension probes, the probability of mechanical dehybridization is loading rate-dependent. Therefore, to fully realize the potential of TaCT, future investigations into the precise loading rate and force duration of mechanoreceptors is required and this needs to be coupled with the development of TaCT probes with different lengths and GC%. TaCT signal reports the total number of mechanical events exceeding F_{peel}, which is orthogonal to biochemical analysis using antibodies and nucleic acids. The limit of detection of TaCT is akin to any other flow cytometry assay and depending on the instrumentation and staining procedures is likely capable of detecting 100s of probes per cell. If greater force magnitude detection is desired, duplexes with greater F_{peel} should be designed. In applications that use TaCT to characterize mechanically active cells, it is important to include a cholesterol strand uptake calibration to account for potential cholesterol insertion differences between different cell types. A negative control that is not mechanically active should also be included to account for background uptake of cholesterol strands. Taken together, TaCT will open up a new class of tools for mechanobiology potentially allowing one to link single-cell mechanical phenotype with other biochemical properties.

Methods

This research complies with all relevant ethical regulations.

1. Simulation of DNA peeling

The dsDNA peeling was modeled with oxDNA by adding harmonic traps (effectively springs) to two terminal nucleotides of a DNA stand (Figure S1). Each trap was assigned with a stiffness constant of 11.42 pN/nm, and one of the traps was moved at a given rate (loading rate = 2.81×10^3 nm/s) with respect to the other fixed trap. The effective stiffness constant of the two traps in series can be calculated using:

$$1/k_{eff} = 1/k_1 + 1/k_2$$

where k_1 and k_2 are the stiffness constants of the two traps and k_{eff} is the effective stiffness constant. The k_{eff} of the system is calculated to be 5.71 pN/nm. The total displacement of the two terminal nucleotides from the respective trap centers is defined as net displacement. Force is then calculated by multiplying k_{eff} with net displacement projected along the force axis (z - axis). This force is plotted against the net displacement with an exponential moving average (EMA) of data points. The oxDNA model considers base pairs as broken when the pairing energy is less than 10% of that of a fully formed base pair. The critical force at which peeling occurs (F_{peel}) is defined here as the force at which the total number of base pairs falls to ≤5. The first 100 data points were averaged (to reduce the stochasticity in simulation data) to obtain the value of F_{peel}. Modeling parameters were adopted from published literature and from examples available at dna.physics.ox.ac.uk website.[1]

2. Oligonucleotide preparation

Conjugation with dyes—The load-bearing strand was conjugated with Cy3B NHS on the internal amine, the 24mer peeling strand was conjugated with Atto647N NHS on the 5’ amine, and the TGT bottom strands were conjugated with Cy3B (Table S2). Briefly, an excess amount of NHS dye (50 μg) was dissolved in DMSO immediately before use and then reacted with 10 nmol amine oligonucleotide at room temperature for 1 h in 1×PBS containing 0.1 M $NaHCO_3$. The mixture after reaction was desalted with P2 gel and purified with an HPLC coupled to an Advanced oligonucleotide C18 column (Figure S2). The product was eluted in Solvents A: 0.1 M TEAA and B: acetonitrile with linear gradients of 10–35% Solvent B over 25 min and 35–100% Solvent B over 5 min at 0.5 mL/min flow rate, and dried in a Vacufuge overnight. The dried oligo-dye conjugate was reconstituted in water and the concentration was determined by its absorbance at 260 nm with Nanodrop.

Conjugation with cRGD—Maleimide-cRGDfk was used for conjugation with thiol oligonucleotide strand (load-bearing strand). Briefly, 5 nmol of thiol oligonucleotide was reduced in 200× molar excess TCEP at room temperature for 15 min, and the mixture was added to 0.5 mg (excess) of maleimide-cRGDfk in 1×PBS (pH = 6.8) to react at room temperature for 1 h. The reaction mixture was then desalted with P2 gel and purified by HPLC with advanced oligonucleotide column as described above.

For alkyne oligonucleotide TGT top quencher strand, azide-RGD was first prepared and then conjugated to the oligo. Briefly, excess amount of azide-NHS (~0.5 mg) was used to react with 100 μg cyclic (RGD)fk-PEG2-amine overnight at 4 °C. The product was purified with HPLC coupled to a Grace C18 column for peptide purification. Product was eluted in Solvents A: 0.1% TFA in H_2O and B: 0.1% TFA in ACN with linear gradients of 10–40% Solvent B over 30 min and 40–75% Solvent B over 10 min at 1 mL/min flow rate. The purified product was dried in a Vacufuge overnight. Stock solutions of $CuSO_4$ (20 mM in water), THPTA [Tris(3-hybroxypropyltriazolyl methyl)amine] (50 mM in water), and sodium ascorbate (100 mM in water) were prepared. A final mixture of 100 μM azide-RGD, 50 μM of alkyne-DNA, 0.1 mM $CuSO_4$, 0.5 mM THPTA, and 5 mM sodium ascorbate in 1X PBS was allowed to react at room temperature for 2 h. The product was purified by P2 gel, followed by HPLC with advance oligonucleotide column as described above.

3. DNA substrates preparation

Amine glass slides—Glass slides (25 × 75 mm) were placed on a Wash-N-Dry rack, rinsed with water (18.2 MΩ), and sonicated in ethanol and water for 15 min each, followed by 6 rinses with water. Fresh piranha solution was made by mixing concentrated sulfuric acid and hydrogen peroxide (30%) at a 3:1 ratio (v/v) in a total volume of 200 mL and added to the slides for etching. CAUTION: PIRANHA SOLUTION IS HIGHLY REACTIVE AND MAY EXPLODE IF MIXED WITH ORGANIC SOLVENTS. Next, the slides were rinsed again with copious amount of water to remove the acid, and then rinsed in ethanol to remove water. Then, 200 mL of 3% APTES in ethanol was prepared and added to the glass slides at room temperature to react for 1 h for amine modification. After reaction, the glass slides were washed with copious amounts of ethanol, and bake dried in an oven (80 °C) for 20 min. The amine modified glass slides were stored at −20 °C until use.

Biotin substrate preparation—An amine modified glass slide was carefully placed on a parafilm-lined petri dish. Then, 1 mL of 4 mg/mL Biotin-NHS in DMSO was added to the slide and incubated overnight. On the second day, after washing with copious amounts of ethanol and then water several times, the glass slide was air-dried, and attached to an ibidi sticky-slide imaging chamber or a bottomless adhesive 96-well plate. The wells were passivated in 1% BSA in PBS for 10 min at room temperature and then washed with PBS. Streptavidin at 50 μg/mL in PBS was added to each well and incubated for 30 min at room temperature, and the excess was washed away with PBS. Meanwhile, TaCT/peeling probe (load-bearing strand:peeling strand = 1:1.5) was annealed at 50 nM by heating to 95 °C for 5 min and then gradually cooling down to 20 °C in 20 min. For TGT substrates, the BHQ2 top strand was annealed with Cy3B bottom strand (1.1:1 ratio) at 50 nM. Next, the probes were added to each streptavidin-coated well and incubated for 30 min. The excess was rinsed away with PBS before imaging (Figure S3).

4. Probe density calibration

Lipid vesicles—Lipid vesicles were prepared with 100% DOPC or with 99.5% DOPC and 0.5% Texas Red DHPE (TR-DHPE). Lipid was dissolved in chloroform in a round-bottom flask and dried with rotary evaporator and under ultra-high purity N_2 stream. The dried lipids were subsequently resuspended in Nanopure water at 2 mg/mL and endured three freeze/thaw cycles in acetone and dry ice bath or 40 °C water bath. Lipids were then extruded ten times through a high-pressure extruder assembled with a 0.2 μm membrane to obtain uniform vesicles.

Supported lipid bilayer preparation—A glass bottom 96-well plate was used for preparing supported lipid bilayers. Each well was filled and soaked with ethanol for 15 min and rinsed with 5 mL Nanopure water. Subsequently, 200 μL of 6 M NaOH solution was added to each well for base etching at room temperature for 1 h. After washing each well with 10 mL Nanopure water, lipid mixtures containing different percentage of TR-DHPE vesicles (0.01%−0.5%) were added at 0.5 mg/mL in PBS to coat the glass surfaces for 20 min. After the lipid vesicles fused to the surfaces, the wells were rinsed with 10 mL water and 10 mL PBS and imaged with a fluorescence microscope to create a standard curve for probe density calibration.

Solution phase standard curve preparation—Surfaces were first washed with ethanol and water and passivated with 1% BSA to prevent any surface adsorption. Different concentrations of TR-DHPE (2.96 nM – 740 nM) and a series of Cy3B-oligo solutions (10 nM – 500 nM) were then added to each well and their bulk fluorescence intensity in solution was measured with a fluorescence microscope (4 μm above surface) to create a standard curve (Figure S4).

5. Cell culture and transfection

NIH3T3 cells (ATCC, CRL-1658) were cultured in DMEM (10% CCS, 1% P/S) at 37 °C with 5% CO_2. MEF and MEF vinculin null cells were obtained from the Garcia Lab at Georgia Tech and cultured in DMEM (10% FBS, 1% P/S) at 37 °C with 5% CO_2. Cells were passaged at 80% confluency every two days by detaching using trypsin and replating at lower density. For MEF vinculin null cells, a plasmid encoding full-length vinculin and GFP was used for transfection. Cells were seeded in a 6 well plate and transfected with 0, 0.25, 0.5, 2, or 3 μg of the plasmid for 24 h. The expression was validated by flow cytometry (Figure 2I).

6. Mouse platelets

Blood of C57Bl/6J mice were collected after cardiac puncture or via retro-orbital plexus, and anticoagulated with acid-citrate-dextrose. After mixing with equal volume of Tyrode's buffer (140 mM NaCl, 2.7 mM KCl, 0.4 mM NaH_2PO_4, 10 mM $NaHCO_3$, 5 mM Dextrose, 10 mM HEPES, 3U apyrase), mouse platelets were isolated by centrifugation at 200×g for 5 min and subsequently supplemented with 1U apyrase and 1 μM prostaglandin E1. Finally, the mouse platelets were spun down at 700×g for 5 min and resuspended in Walsh buffer (137 mM NaCl, 2.7 mM KCl, 1 mM $MgCl_2$, 3.3 mM NaH_2PO_4, 20 mM HEPES, 0.1% glucose, 0.1% bovine serum albumin, pH 7.4) at a density of ~1×10^9 platelets per mL.

7. Fluorescence microscopy

Integrin tension imaging—Imaging was conducted with a Nikon Ti2-E microscope. All the fibroblast cells were plated onto the DNA probe substrates in DMEM (10% serum, 1% P/S) and allowed to attach for 15–20 min in the incubator at 37 °C in medium. Then, the cells were allowed to further spread at room temperature and imaged up until 60 min after plating in RICM, Cy3B, and Atto647N channels with accommodating filter settings and a sCMOS detector.

Mouse platelets were plated onto the DNA probe substrates in 1× Tyrode's buffer (134 mM NaCl, 12 mM $NaHCO_3$, 2.9 mM KCl, 0.34 mM NaH_2PO_4, 5 mM glucose, 5 mM HEPES, 0.1% BSA, pH 7.4) supplemented with 2 mM $CaCl_2$, 1 mM $MgCl_2$, and 10 μM ADP, and imaged at room temperature up until 60 min after plating in RICM, Cy3B, and Atto647N channels.

Immunostaining—Cells incubated on DNA probe substrates were fixed in 4% formaldehyde for 10 min, followed by two gentle PBS washes and permeabilization with 0.1% triton X-100 in PBS for 10 min. The cells were then blocked in 1% BSA for 1 h and then stained. Fixed cells were incubated with primary antibodies (anti-YAP: 2

μg/mL, anti-pFAK Y397: 5 μg/mL in 1% BSA) at 4 °C overnight. After rinsing three times with PBS, cells were incubated in secondary antibody (2 μg/mL in 1% BSA) for 1 h at room temperature. For actin straining, fixed cells were incubated with 0.5 μM SiR-actin or phalloidin iFluor 647 (1:1000 dilution). Microscopy images were acquired with accommodating filter settings.

8. Flow cytometry

For all fibroblast cells, 1×10^4 cells were seeded on the TaCT substrate and collected by gentle scraping 60 min after seeding. After spinning down and washing in PBS containing 5 mM EDTA, the collected cells were resuspended in DPBS (without Ca^{2+} and Mg^{2+}, with 5 mM EDTA) and immediately run through a flow cytometer for TaCT analysis.

For mouse platelets, 3 μL of the platelets were diluted in 600 μL 1× Tyrode's buffer. 100 μL platelets were then added to the TaCT substrate with different supplements (Ca^{2+}, Mg^{2+}, ADP, Mn^{2+}). After 1 h, platelets were collected by pipetting them off from the substrate and then washed before running through flow cytometer for TaCT analysis.

9. Data analysis

Tension imaging data—All representative microscopy images were repeated collected and confirmed from at least 3 independent replicates. All microscopy data was analyzed with Image J software.

For quantification of FRET efficiency, Cy3B load-bearing strand and Atto647N peeling strand were annealed and immobilized on a biotin substrate and imaged to obtain the fluorescence intensity with both donor and acceptor present (I_{DA}). Similarly, Cy3B load-bearing strand and amine peeling strand were annealed and immobilized on a biotin substrate and imaged to obtain fluorescence intensity when only the donor was present (I_D). After sCMOS background subtraction of the images, the fluorescence intensity in Cy3B was averaged from 5 different positions of the substrates. The FRET efficiency was calculated with the equation $1 - I_{DA}/I_D$.

The probe density was estimated as described previously in literature[2]. Briefly, peeling probe and TGT substrates with unquenched Cy3B fluorescence strand were prepared. A calibration curve was made with fluorescent supported lipid bilayers (SLB) to provide a count for molecules/μm^2, and the F-factor was calculated using a standard curve with a series of Cy3B concentrations (Figure S4). The average intensity of three substrates was used to calculate the probe density using the calibration curve.

Microscopy images of integrin tension was presented in formats including raw data, background subtracted or normalized molecular tension images, and %peel/%rupture. For quantitative analysis of microscopy data with cells, the sCMOS background was subtracted, and the fluorescence intensity (mean±SD) of the substrate background was used as a threshold. Raw integrated intensity, contact area, and tension area of the ROIs of the cells were measured and plotted. The tension signal in Cy3B for each image was used to calculate the %peel or %rupture according to literature (Figure S10) [2].

Flow cytometry data—Flow cytometry data was analyzed with Flowjo software. Briefly, the debris and aggregated cells were gated out by first identifying the live cells using the forward scatter and side scatter area and then the singlet cells using the forward and side scatter height (Figure S10). Following gating, the fluorescence signal of each viable singlet cell in the Atto647N channel and Cy3B channel was measured and analyzed. The signal intensity was presented in histograms, and the median fluorescence intensity (MFI) or geometric mean fluorescence intensity (gMFI) was used for comparison between groups. The %positive cells was determined by creating a vertical gate in the histogram of the negative control group so that ~99.5% of cells in the negative control had a lower fluorescence than the gate. We anticipate that TaCT has a similar detection limit to any other flow cytometry assays.

Extended Data

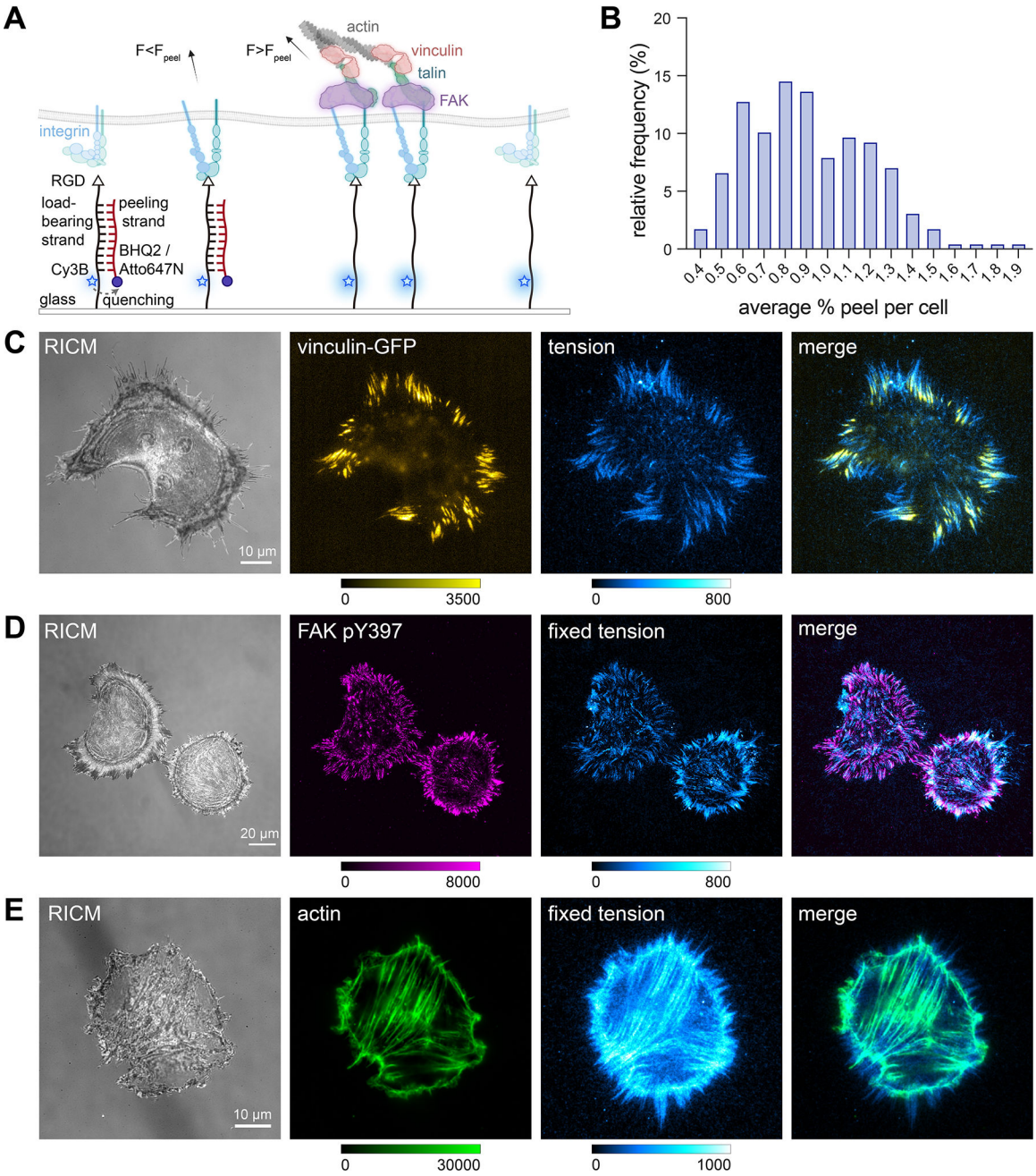

Extended Figure 1. Mapping integrin forces with peeling probe.

(A) Scheme showing that when integrin is in the inactive state, the peeling probe remains in the duplex form. As integrin binds and pulls on the RGD ligand, if $F<F_{peel}$, the peeling strand is intact, and if $F>F_{peel}$, the duplex dehybridizes and the Cy3B fluorescence turns on. FA proteins such as vinculin, talin, and FAK, as well as actin cytoskeleton participate intensively during the integrin force generation and mechanotransduction. (B) Histogram of 227 NIH3T3 cells showing the distribution of average % peel/μm^2 per cell after 1 h incubation on peeling probe substrate. Data acquired from 3 biological replicates, bin

width = 0.1%. (C) Representative microscopy images show that GFP-vinculin colocalized with integrin tension signal. Images were acquired with MEF GFP-vinculin cells that were cultured on peeling probe substrate. (D) Representative microscopy images show that the phosphorylated FAK (pY397) colocalized with fixed integrin tension signal. MEF cells were incubated on peeling probe substrate for 40–45min, fixed and stained with Rabbit anti-FAK pY397 and Alexa488 labeled secondary antibody, followed by imaging. (E) Representative microscopy images show that the actin stress fibers colocalized with fixed tension signal. MEF cells were incubated on peeling probe substrate for 60–90 min, fixed and stained with Alexa647-phalloidin, followed by imaging.

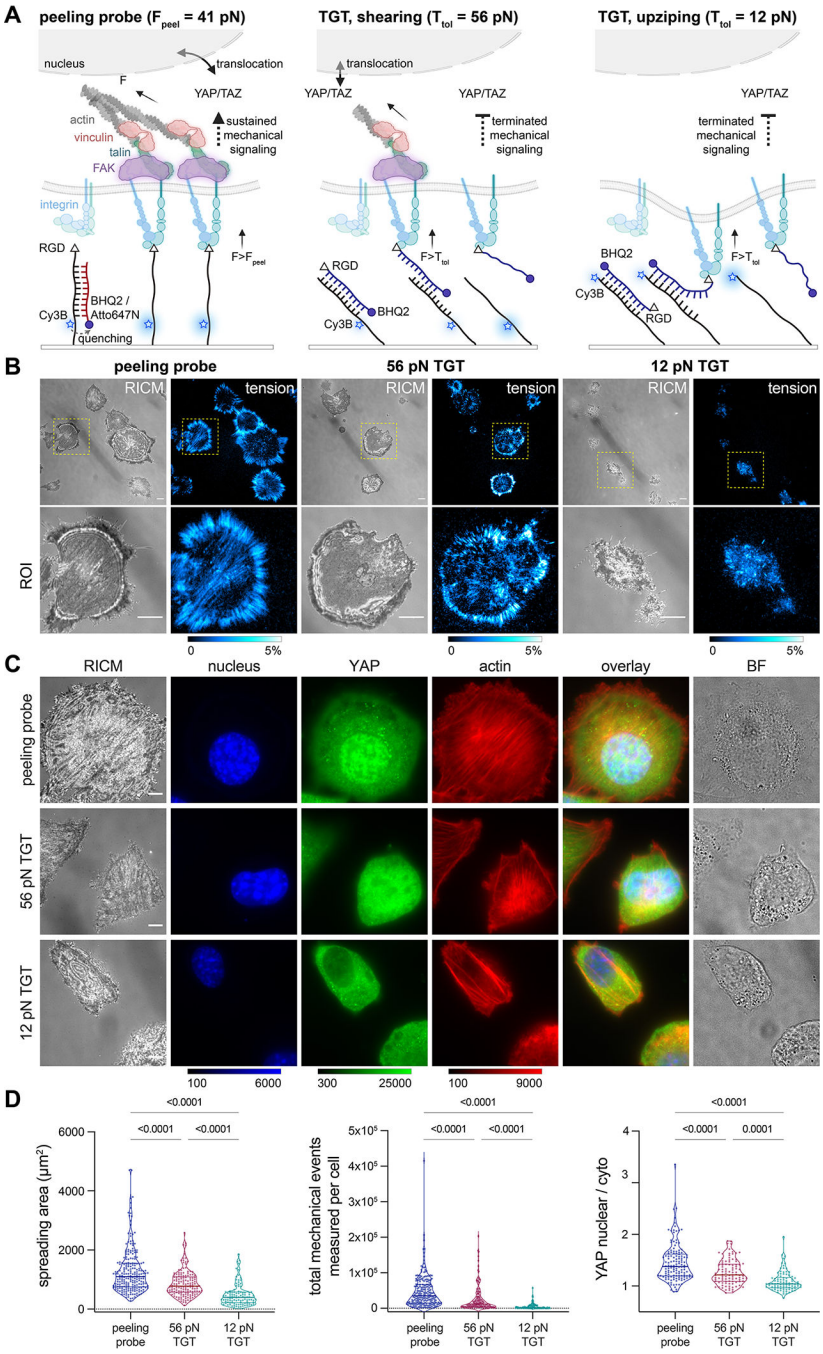

Extended Figure 2. Peeling probe does not perturbate mechanotransduction unlike TGTs.

(A) Schematics comparing the mechanism of TaCT/peeling probe and TGTs. Peeling probe maps integrin tension greater than 41 pN as the BHQ2 strand is separated, and the RGD anchor remains despite the duplex dehybridization. In contrast, TGTs map integrin forces greater than 56 or 12 pN in the shearing or unzipping geometry. The force-induced rupture of the duplex generates a Cy3B turn-on fluorescence signal as the top BHQ2 strand separates from the Cy3B anchor strand. Unlike peeling strand, the loss of the RGD anchors in TGTs terminates mechanotransduction through integrins. (B) Representative microcopy

images of NIH3T3 cells incubated on peeling probe or TGT substrates for ~45–60 min. Second row of images show the zoom-in view of the ROIs marked with the yellow dashed box. Intensity bar for Cy3B image indicates the peeling/rupturing percentage of the probes. (C) Microscopy images of NIH3T3 cells incubated on peeling probe or TGT substrates for ~90 min, fixed and stained for nucleus (DAPI), actin (SirActin), and YAP (Alexa488 conjugated antibody). Scale bar = 5 μm. Intensity bar indicates the grey value. (D) Quantitative analysis of the spreading area, %peel or %rupture, and YAP translocation for NIH3T3 cells incubated on three substrates for 60 min. For spreading area and tension quantification, data was collected from 3 biological replicates (n = 227, 150, and 105 for cells on peeling probe, 56 pN TGT, and 12 pN TGT substrate). For analysis on YAP translocation, images in DAPI channel were used as masks to quantify the mean fluorescence intensity of nuclear YAP and cytoplasm YAP. Data was acquired from 3 biological replicates (total n = 134, 98, and 86 cells for peeling probe, 56 pN TGT and 12 pN TGT substrate). Plots show lines at the median and interquartile values. Statistical analysis was performed with one-way ANOVA and Tukey’s multiple comparison test.

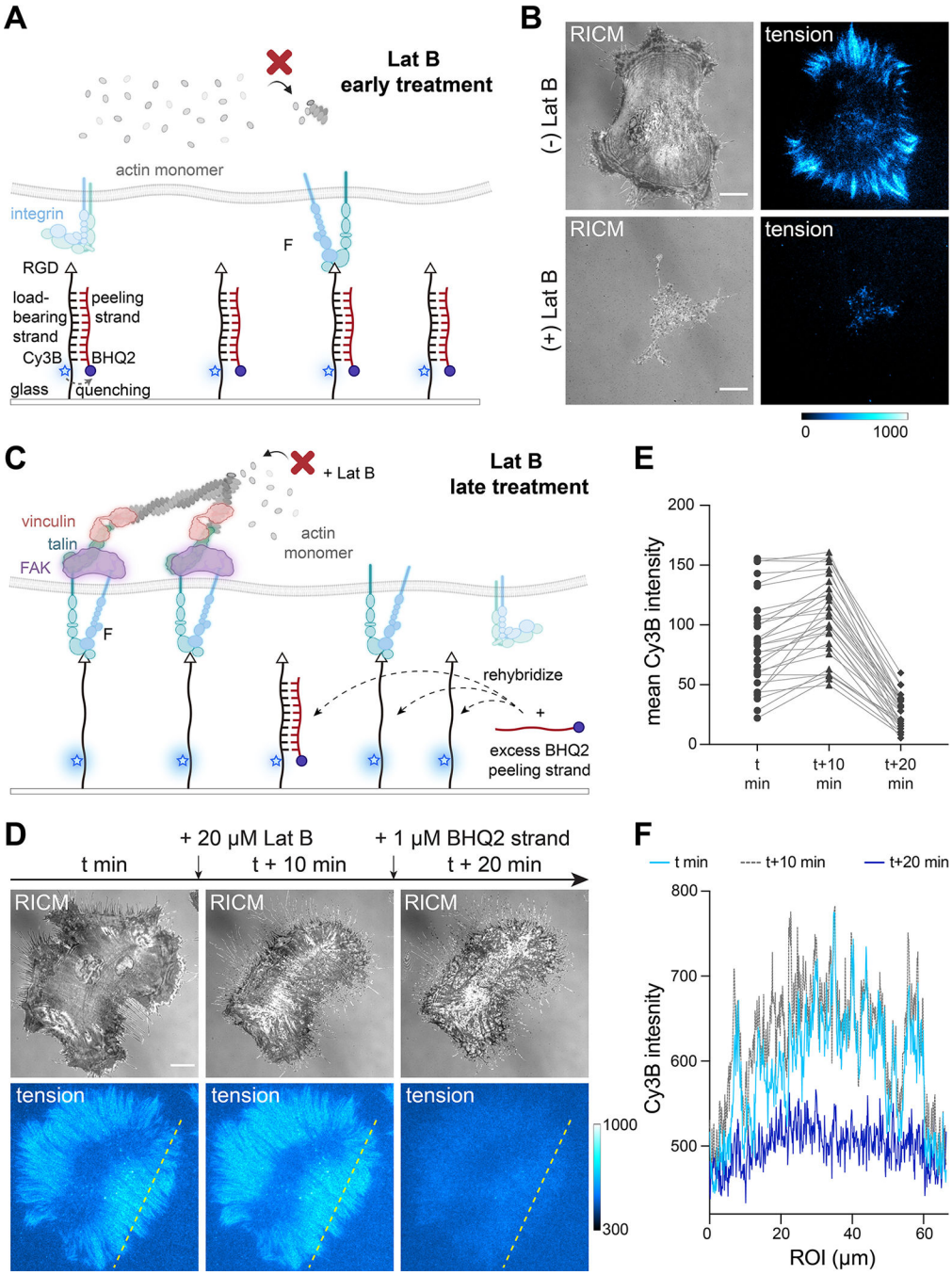

Extended Figure 3. Lat B inhibition of cells.

(A) Scheme showing that Lat B early treatment inhibits integrin force generation by inhibiting actin polymerization. (B) Representative RICM and Cy3B microscopy images of MEF cells incubated on peeling probe substrate after early Lat B treatment. Cells were treated with 20 μM Lat B after 15 min of plating on the substrate and imaged after 45 min of incubation. (C) Scheme showing that when integrin force signals are already generated on peeling probe substrate, if the force transmission is terminated by late Lat B treatment, with additional BHQ2 peeling strand the peeling probe can rehybridize to the duplex form.

(D) Representative RICM and raw Cy3B microscopy images of MEF cells treated with 20 μM Lat B 50 min after seeding. The tension signal remained after 10 min of Lat B treatment and diminished after the addition of excess BHQ2 peeling strand. (E) Quantitative analysis of tension signal changes after Lat B treatment and the addition of BHQ2 peeling strand in n = 30 cells. (F) Linescan of the ROI (yellow dashed line) in (D) before Lat B treatment, with Lat B treatment, and with excess BHQ2 peeling strand.

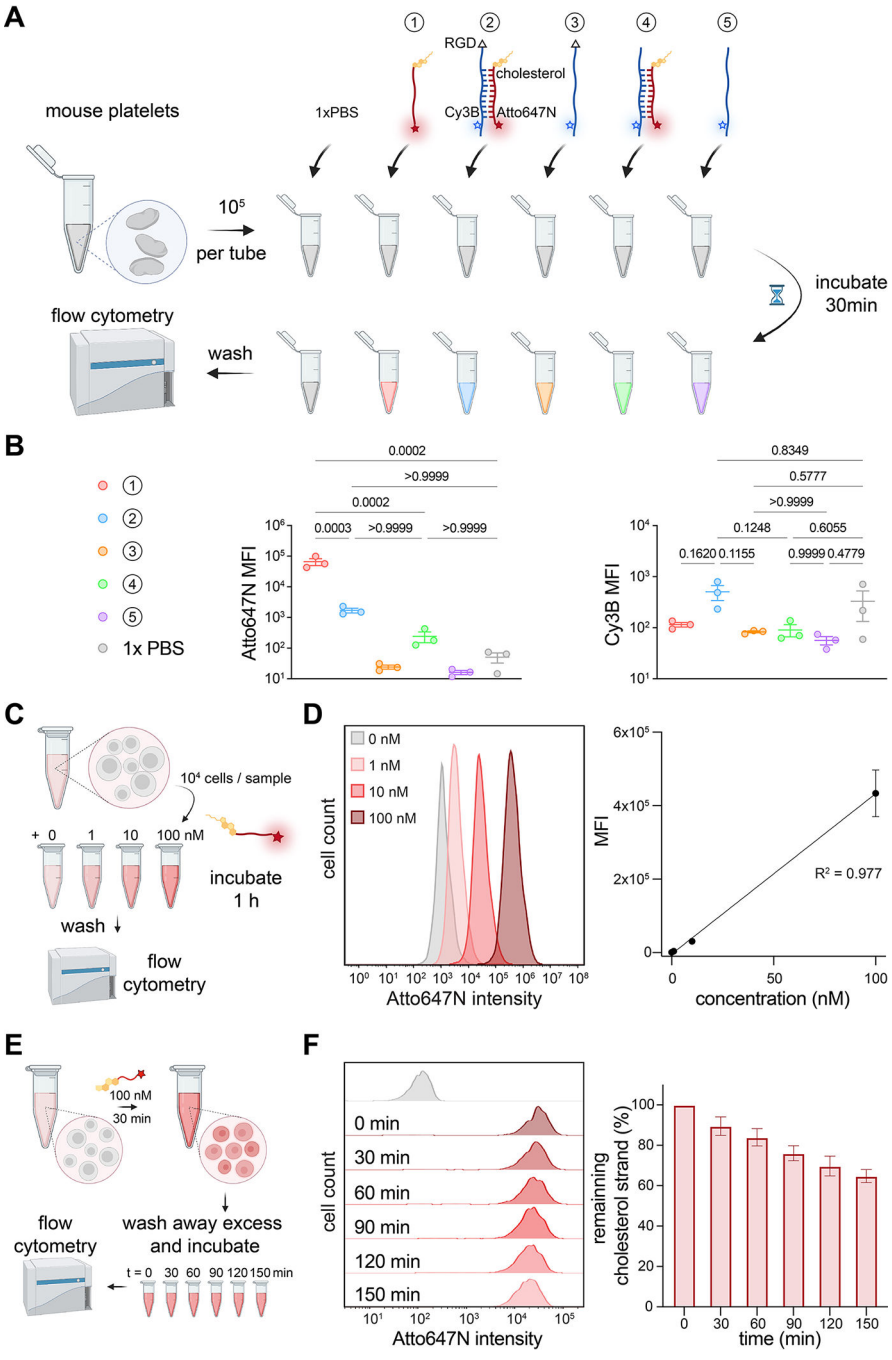

Extended Figure 4. Cholesterol DNA strands association and dissociation in cells.

(A) Scheme showing flow cytometry measurements of the DNA strands uptake in solution. Mouse platelets were incubated with 50 nM of cholesterol peeling strand, TaCT duplex, load-bearing strand, TaCT duplex lacking RGD, and load-bearing strand lacking RGD in Tyrode's buffer for 30 min and spun down three times to wash away the excess oligos. The association was measured in both Atto647N and Cy3B channels by a flow cytometer. (B) Cy3B and Atto647N median fluorescence intensity (MFI) of platelets incubated with different oligonucleotides. Data collected from 3 replicates (mean±SEM). Statistical analysis was performed by one-way ANOVA and Tukey's multiple comparison. (C) Scheme showing flow cytometry measurements of the concentration dependent incorporation of cholesterol peeling strand. MEF cells were incubated with 0, 1, 10, and 100 nM of cholesterol peeling strand for 1 h. The excess cholesterol peeling strand was washed away by spinning down in PBS three times, and the fluorescence intensity of cells was measured by a flow cytometer. (D) Representative histogram of cholesterol peeling strand association in cells. Atto647N MFI was plotted from 3 replicates (mean±SD). Linear relationship between cholesterol strand concentration and cell association was found, $R^2 = 0.977$. (E) Scheme showing the measurement of cholesterol peeling strand dissociation from the cell. NIH3T3 cells were incubated with 100 nM cholesterol peeling strand for 30 min and rinsed with PBS 3 times. Cells were divided into 6 aliquots and the remaining cholesterol strand in cells was measured every 30 min for 150 min by flow cytometry. (F) Representative histogram shows the decay of fluorescence in cells over time. The normalized MFI from 2 replicates was plotted to show the dissociation of cholesterol strand over time in NIH3T3 cells (mean±SD).

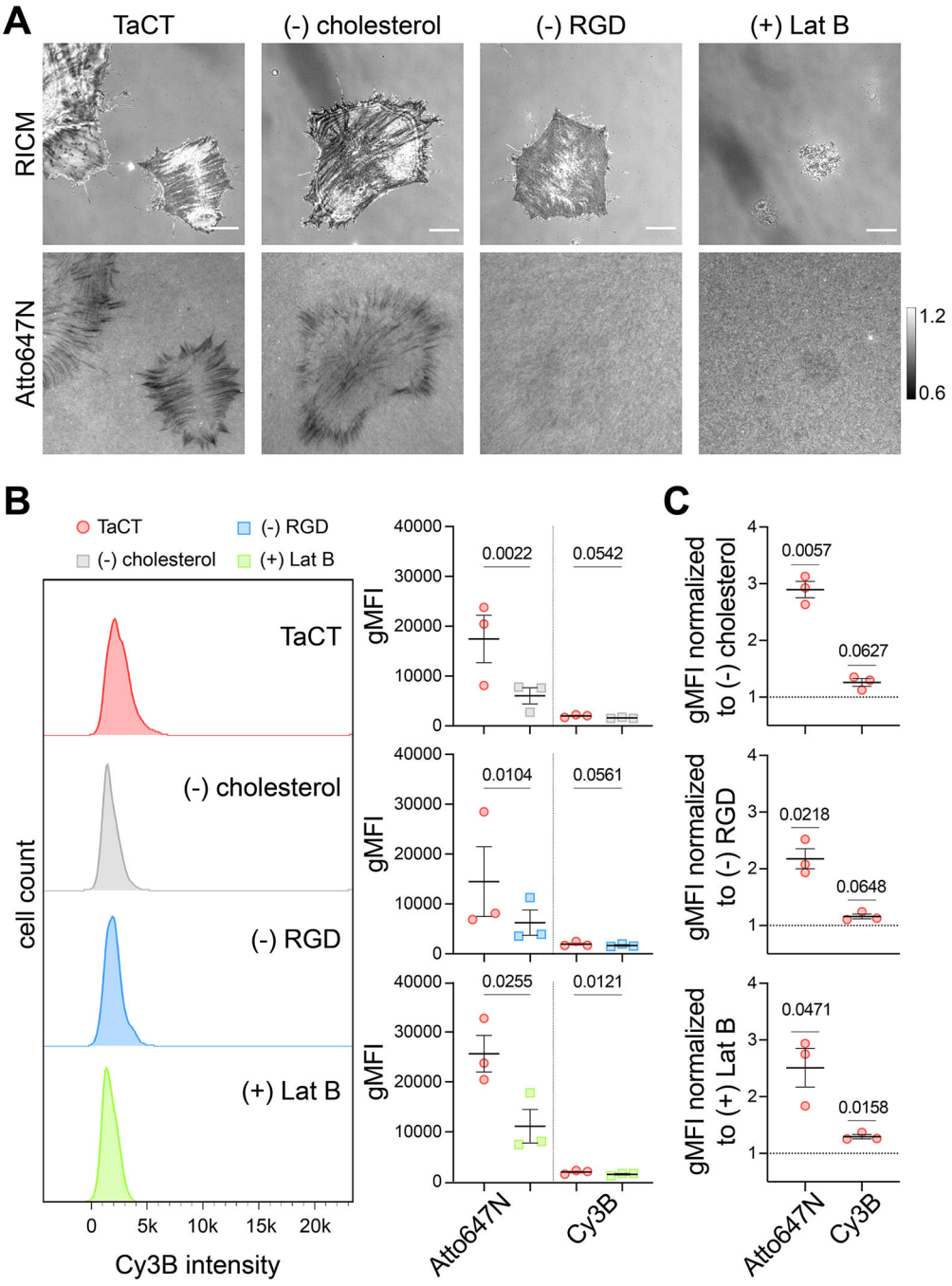

Extended Figure 5. Control experiments supporting the concept of TaCT.

(A) Representative microscopy images of NIH3T3 cells cultured on TaCT substrate, or control substrate lacking cholesterol, lacking RGD, or treated with Lat B. Atto647N shows the signal normalized to the background intact probes. Scale bar = 10 μm. (B) Representative flow cytometry histograms show that NIH3T3 cells in TaCT, (−)cholesterol, (−)RGD, and (+)Lat B groups had indistinguishable Cy3B intensity. Quantitative analysis (mean±SEM) shows that cells cultured on TaCT substrate had similar level of geometric mean fluorescence intensity (gMFI) compared to control groups in Cy3B channel, despite

higher Atto647N gMFI. Data collected from 3 replicates for each control, and statistical analysis was performed using ratio paired two-tailed student's t-test. (C) Plots show the gMFI of cells after TaCT normalized to different controls in both Atto647N and Cy3B channels (n = 3, mean±SEM). One sample t-test was used for statistical analysis to test whether TaCT signal is significantly different in Atto647N and Cy3B compared to a hypothetical value of 1 (representing no TaCT signal in the corresponding control group). TaCT signal in Atto647N channel consistently provides 2 to 3 fold higher gMFI.

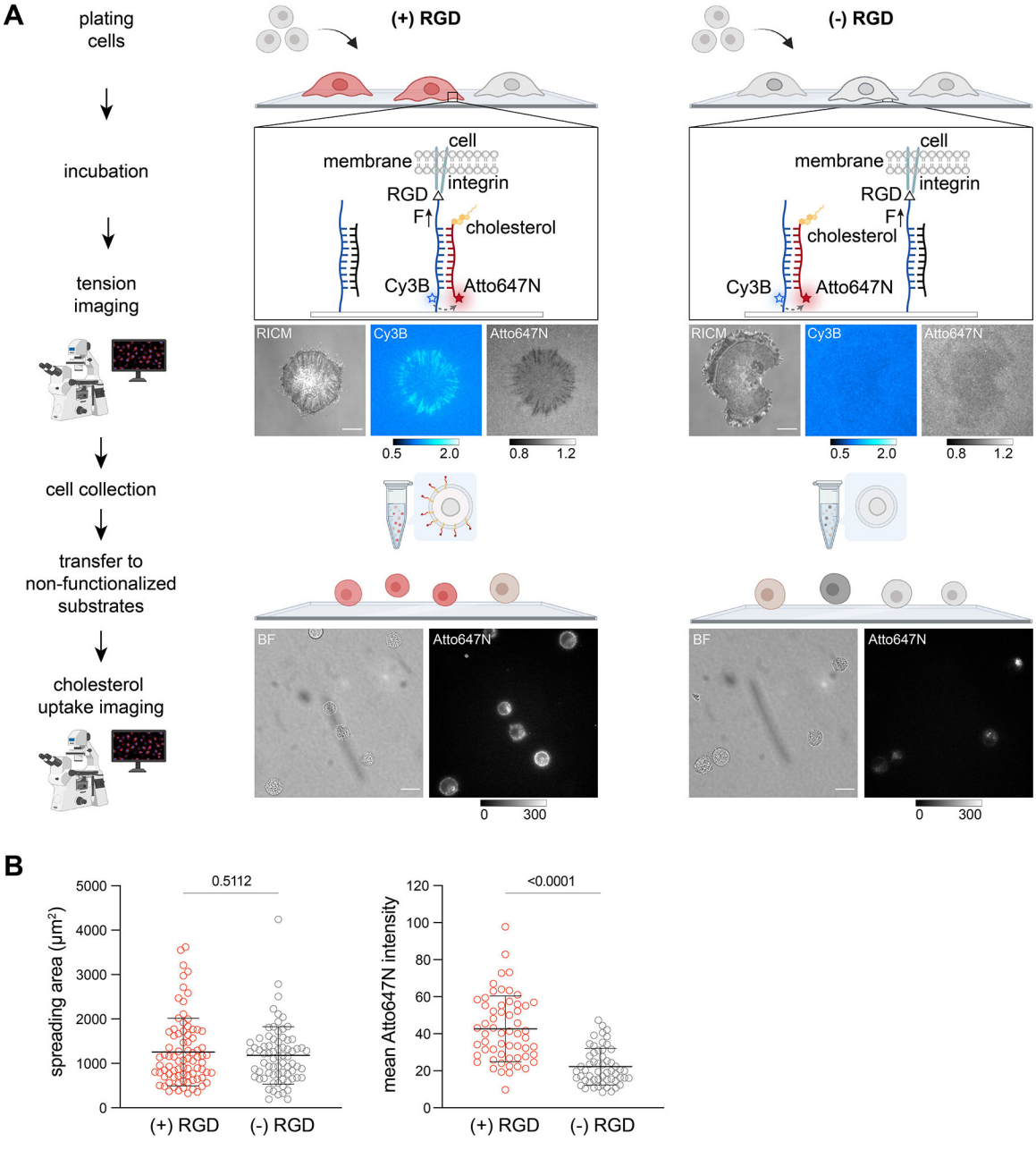

Extended Figure 6. Spreading control for TaCT.

(A) Scheme and representative microscopy data showing that TaCT signal is not due to spreading of the cells on the substrate. NIH3T3 cells were incubated on a TaCT substrate doped with a non-fluorescent DNA duplex, or a TaCT substrate lacking RGD doped with a non-fluorescent DNA duplex presenting the RGD motif, and imaged 45 min - 60 min after seeding. After confirming the cell spreading, cells were collected, rinsed, and added to non-fluorescent glass substrate to image the cholesterol peeling strand incorporation in the cells. Tension images were normalized to the background of intact probes. Scale bar = 10 μm. (B) Quantitative analysis of the cell spreading area (n=82 and 74 cells) and cholesterol peeling strand incorporation (n=58 and 56 cells) for cells incubated on TaCT (+)RGD or (−)RGD substrates. Data was collected from three replicates and statistical analysis was performed using two-tailed student's t-test.

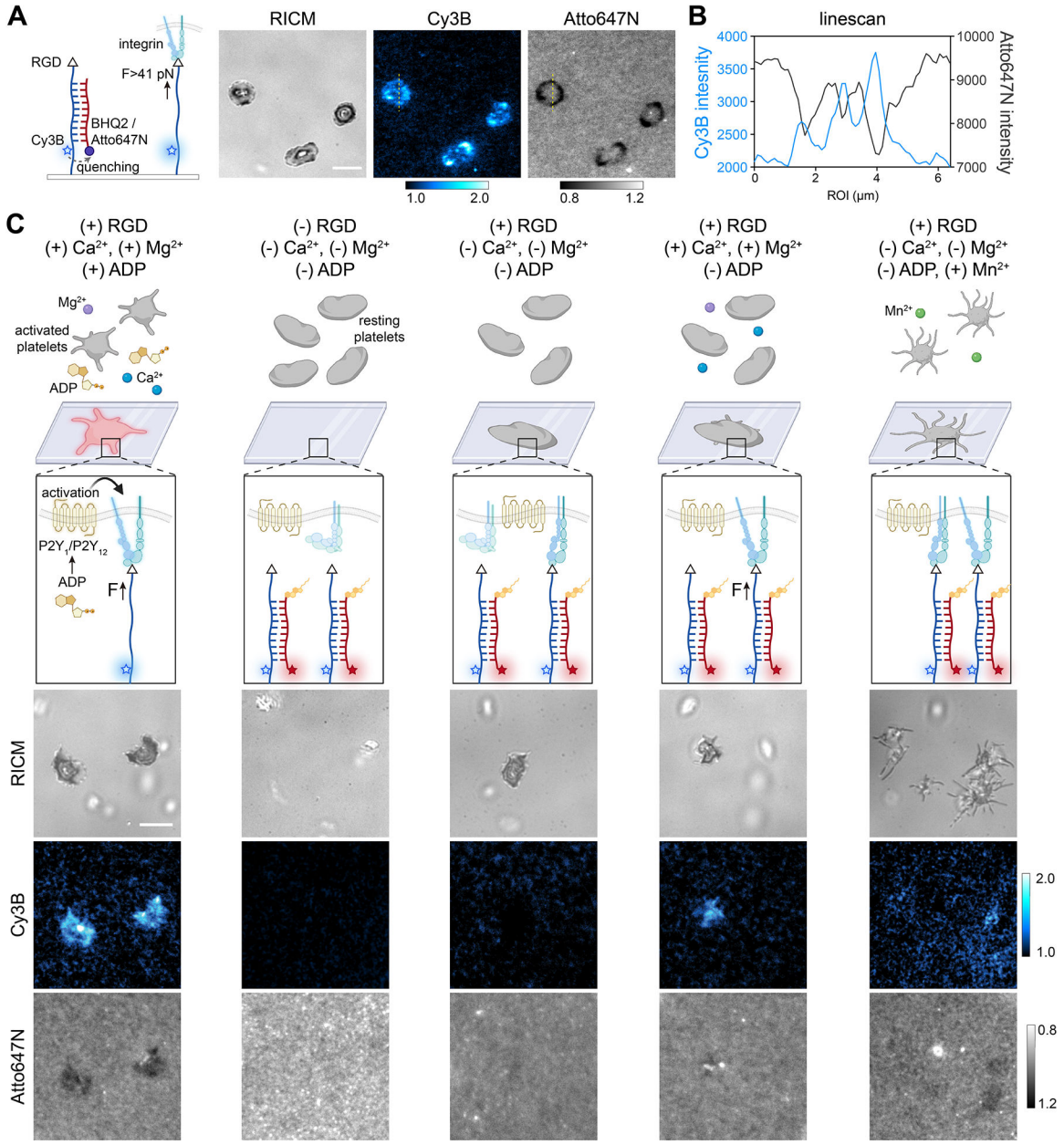

Extended Figure 7. TaCT in Platelets.

(A) Scheme and representative microscopy images showing tension mapping with peeling probe in mouse platelets. Tension images were normalized to the background of intact peeling probes, scale bar = 5 μm. (B) Linescan of the ROI (yellow dashed line) shows anti-colocalization of Cy3B and Atto647N intensities from raw data. (C) Scheme and representative images show mouse platelets incubated on the TaCT substrate in different buffer conditions. RGD, Ca^{2+}, Mg^{2+}, and ADP leads to platelets activation, and withholding any of them results in no/impaired activation. Tension images were normalized to the background of intact TaCT probes, scale bar = 5 μm.

Supplementary Material

Refer to Web version on PubMed Central for supplementary material.

Acknowledgements

K.S. Acknowledges support from the National Institutes of Health (NIH) through NIGMS RM1GM145394, NIGMS R01GM131099 and NIAID AI172452.

Data availability statement

Data summary file contains all individual replicate data from main text, all individual replicate data from supporting information, and all p values from statistical analyses performed are provided in this manuscript at https://osf.io/hkrve/?view_only=cc90b513cb5547358c652e5ace836106.

References

1. Di Carlo D, A mechanical biomarker of cell state in medicine. J Lab Autom, 2012. 17(1): p. 32–42. [PubMed: 22357606]
2. Torrino S and Bertero T, Metabo-reciprocity in cell mechanics: feeling the demands/feeding the demand. Trends Cell Biol, 2022.
3. Evers TMJ, et al. , Reciprocal regulation of cellular mechanics and metabolism. Nat Metab, 2021. 3(4): p. 456–468. [PubMed: 33875882]
4. Belotti Y, et al. , High-Throughput, Time-Resolved Mechanical Phenotyping of Prostate Cancer Cells. Sci Rep, 2019. 9(1): p. 5742. [PubMed: 30952895]
5. Islam M, et al. , Microfluidic cell sorting by stiffness to examine heterogenic responses of cancer cells to chemotherapy. Cell Death Dis, 2018. 9(2): p. 239. [PubMed: 29445159]
6. Lee KCM, et al. , Toward Deep Biophysical Cytometry: Prospects and Challenges. Trends Biotechnol, 2021. 39(12): p. 1249–1262. [PubMed: 33895013]
7. Otto O, et al. , Real-time deformability cytometry: on-the-fly cell mechanical phenotyping. Nat Methods, 2015. 12(3): p. 199–202, 4 p following 202. [PubMed: 25643151]
8. Kozminsky M and Sohn LL, The promise of single-cell mechanophenotyping for clinical applications. Biomicrofluidics, 2020. 14(3): p. 031301. [PubMed: 32566069]
9. Tse HT, et al. , Quantitative diagnosis of malignant pleural effusions by single-cell mechanophenotyping. Sci Transl Med, 2013. 5(212): p. 212ra163.
10. Thery M and Bornens M, Get round and stiff for mitosis. HFSP J, 2008. 2(2): p. 65–71. [PubMed: 19404473]
11. Fletcher DA and Mullins RD, Cell mechanics and the cytoskeleton. Nature, 2010. 463(7280): p. 485–92. [PubMed: 20110992]
12. Sanyour HJ, et al. , Membrane cholesterol and substrate stiffness co-ordinate to induce the remodelling of the cytoskeleton and the alteration in the biomechanics of vascular smooth muscle cells. Cardiovasc Res, 2019. 115(8): p. 1369–1380. [PubMed: 30395154]
13. Guo M, et al. , Cell volume change through water efflux impacts cell stiffness and stem cell fate. Proc Natl Acad Sci U S A, 2017. 114(41): p. E8618–E8627. [PubMed: 28973866]
14. Hang X, et al. , High-Throughput DNA Tensioner Platform for Interrogating Mechanical Heterogeneity of Single Living Cells. Small, 2022. 18(12): p. e2106196. [PubMed: 35322558]
15. Pushkarsky I, et al. , Elastomeric sensor surfaces for high-throughput single-cell force cytometry. Nat Biomed Eng, 2018. 2(2): p. 124–137. [PubMed: 31015629]
16. Yang Z, et al. , The kinetics of force-dependent hybridization and strand-peeling of short DNA fragments. Science China Physics, Mechanics & Astronomy, 2016. 59(8).

17. Cocco S, et al. , Overstretching and force-driven strand separation of double-helix DNA. Physical Review E, 2004. 70(1 Pt 1): p. 011910.
18. Zhang X, et al. , Two distinct overstretched DNA structures revealed by single-molecule thermodynamics measurements. Proceedings of the National Academy of Sciences, 2012. 109(21): p. 8103–8.
19. Snodin BE, et al. , Introducing improved structural properties and salt dependence into a coarse-grained model of DNA. J Chem Phys, 2015. 142(23): p. 234901. [PubMed: 26093573]
20. Zhang Y, et al. , DNA-based digital tension probes reveal integrin forces during early cell adhesion. Nature Communications, 2014. 5: p. 5167.
21. Galush WJ, Nye JA, and Groves JT, Quantitative fluorescence microscopy using supported lipid bilayer standards. Biophys J, 2008. 95(5): p. 2512–9. [PubMed: 18515392]
22. Martino F, et al. , Cellular Mechanotransduction: From Tension to Function. Front Physiol, 2018. 9: p. 824. [PubMed: 30026699]
23. Arnott PM, et al. , Dynamic Interactions between Lipid-Tethered DNA and Phospholipid Membranes. Langmuir, 2018. 34(49): p. 15084–15092. [PubMed: 30350681]
24. You M, et al. , DNA probes for monitoring dynamic and transient molecular encounters on live cell membranes. Nat Nanotechnol, 2017. 12(5): p. 453–459. [PubMed: 28319616]
25. Zhang Y, et al. , Platelet integrins exhibit anisotropic mechanosensing and harness piconewton forces to mediate platelet aggregation. Proceedings of the National Academy of Sciences, 2018. 115(2): p. 325–330.
26. Duan Y, et al. , Mechanically Triggered Hybridization Chain Reaction. Angew Chem Int Ed Engl, 2021. 60(36): p. 19974–19981. [PubMed: 34242462]
27. Ishizaki T, et al. , Pharmacological properties of Y-27632, a specific inhibitor of rho-associated kinases. Mol Pharmacol, 2000. 57(5): p. 976–83. [PubMed: 10779382]
28. Uehata M, et al. , Calcium sensitization of smooth muscle mediated by a Rho-associated protein kinase in hypertension. Nature, 1997. 389(6654): p. 990–4. [PubMed: 9353125]
29. Austen K, et al. , Extracellular rigidity sensing by talin isoform-specific mechanical linkages. Nat Cell Biol, 2015. 17(12): p. 1597–606. [PubMed: 26523364]

Methods-only References

1. Engel MC, et al. , Force-Induced Unravelling of DNA Origami. ACS Nano, 2018. 12(7): p. 6734–6747. [PubMed: 29851456]
2. Zhang Y, et al. , DNA-based digital tension probes reveal integrin forces during early cell adhesion. Nature communications, 2014. 5: p. 5167.

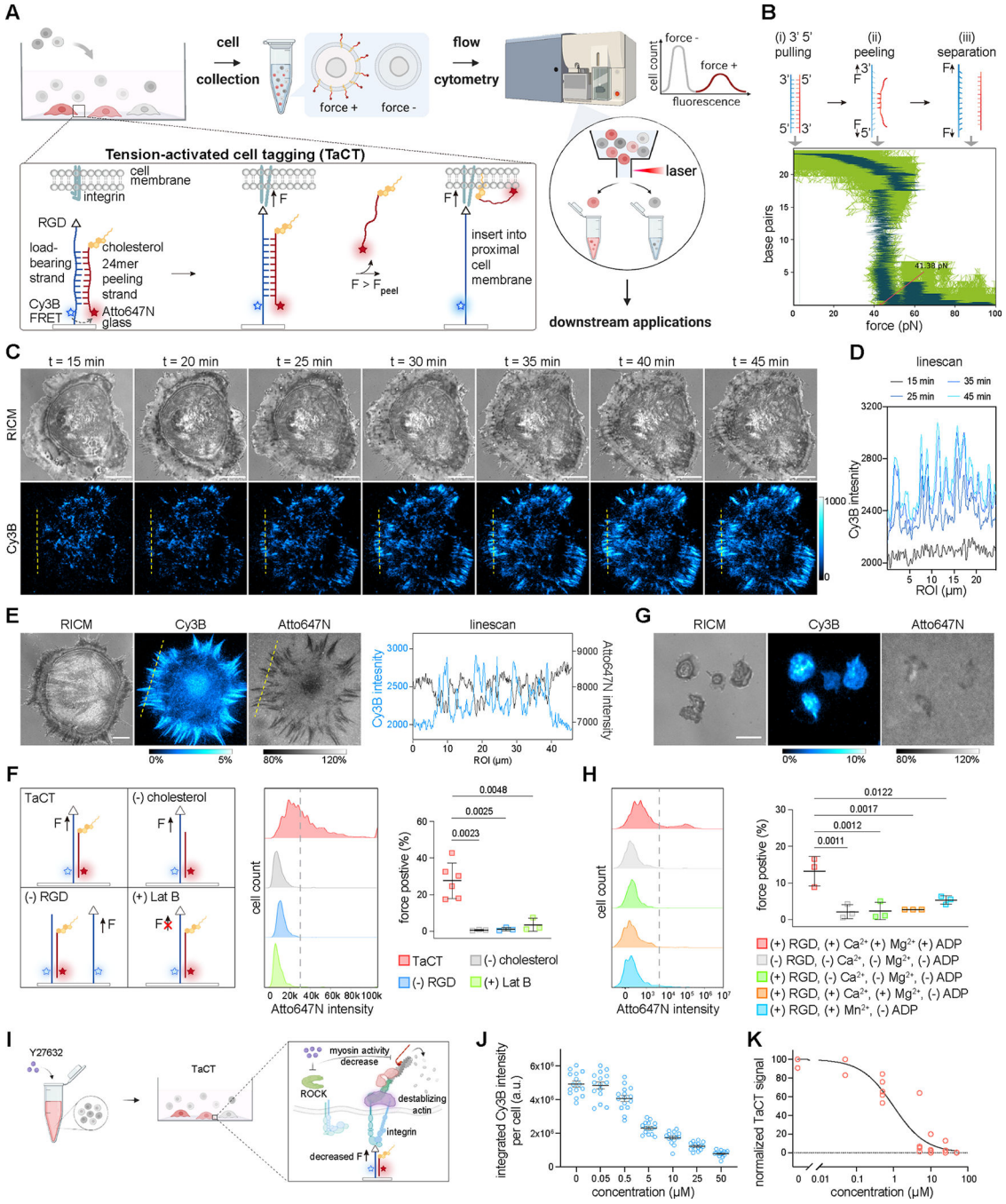

Figure 1. Tension-activated cell tagging (TaCT).

(A) Schematic showing TaCT assay. (B) Plot of 24mer dsDNA stability as a function of applied force generated using oxDNA simulation with a loading rate of 2.81×10^{3} nm/s (shown light green). Dark green shows the exponential moving average (EMA) and indicates a 41pN dehybridization transition. (C) Time-lapse reflection interference contrast microscopy (RICM) and Cy3B fluorescence images of NIH3T3 cell spreading on TaCT surface 15–45 min after seeding. Scale bar = 10 μm. (D) Linescan of Cy3B images noted by yellow dashed line in (C). (E) Representative RICM, Cy3B, and Atto647N

microscopy images of NIH3T3 cell cultured on TaCT substrate. Intensity bar for Cy3B image indicates the % of TaCT probes that undergo force-triggered release while the intensity bar for Atto647N shows the signal normalized to the background of intact TaCT probes. Scale bar = 10 μm. Linescan shows anti-colocalization of Cy3B and Atto647N intensities. (F) Flow cytometry histograms of NIH3T3 cells cultured on TaCT substrates as well as control surfaces with (−)cholesterol, (−)RGD, and (+)Lat B. Plot displays the force positive population from n≥3 biological replicates (mean±SD, two-tailed student's t-test). Grey dashed line indicates the gate for determining force-positive population. (G) Representative RICM, Cy3B, and Atto647N microscopy images of mouse platelets on TaCT substrates. Scale bar = 5 μm. (H) Representative flow cytometry histograms of mouse platelets incubated on TaCT substrates. Grey dashed line indicates the gate for determining force-positive population. Controls included experiments with TaCT probes -RGD (grey), -divalent cations -ADP agonist (green), -ADP agonist (orange), and -ADP/ $+Mn^{2+}$ (blue). Data plotted from n=3 animals (mean±SD, two-tailed student's t-test). (I) Schematic showing Y27632 treatment decreases integrin forces. (J) Quantitative analysis of the integrated Cy3B signal per cell from microscopy images of MEF cells pretreated with 0, 0.05, 0.5, 5, 10, 25, and 50 μM of Y27632 and cultured on peeling probe substrate. Plot shows the result from n=3 biological replicates (mean±SEM). (K) TaCT signal of cells pretreated with different concentration of Y27632. Plot shows the result from n=2–4 biological replicates.

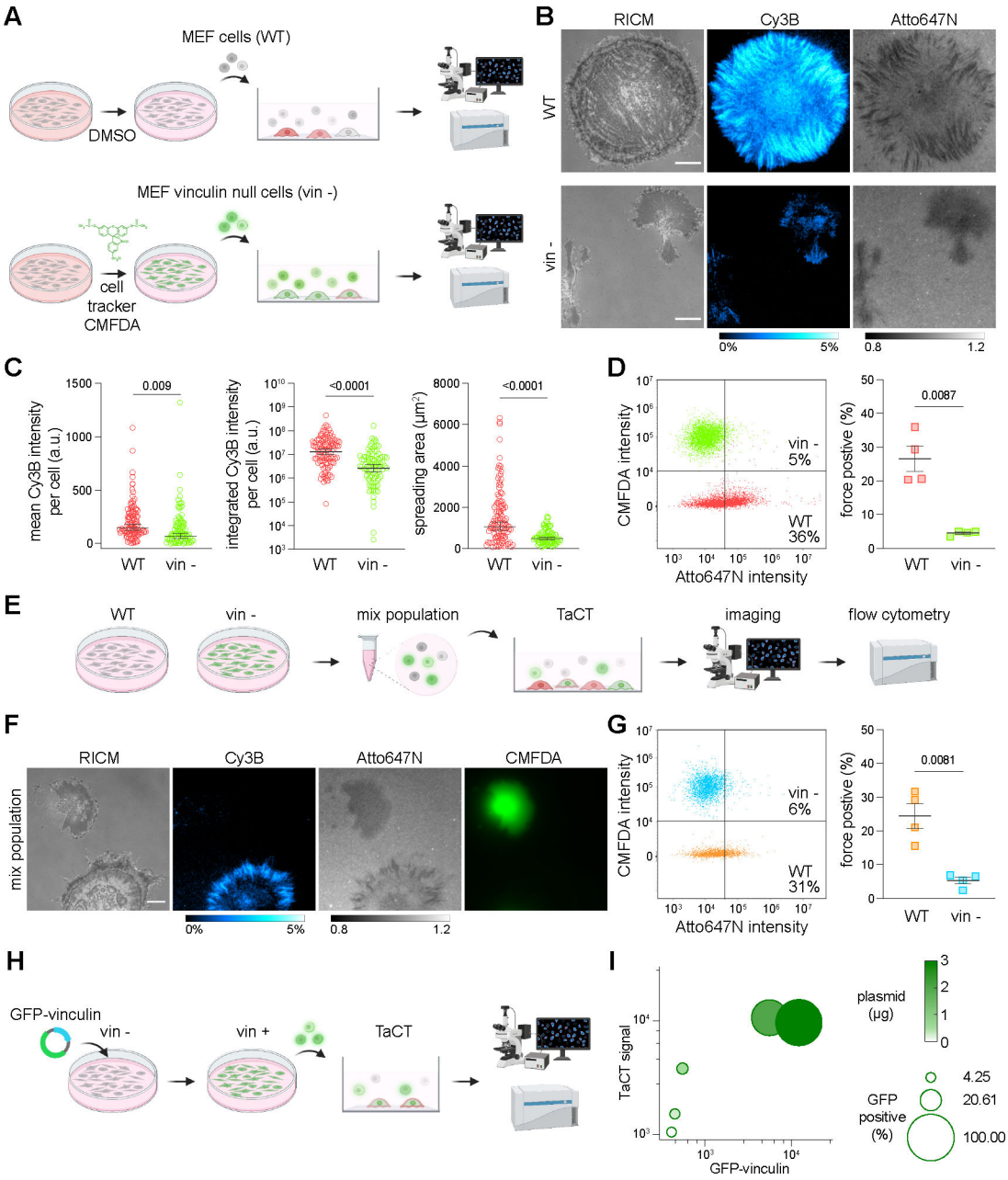

Figure 2. TaCT detecting mechanically active cells in a mixed population.

(A) Schematic shows TaCT workflow for MEF WT and vin- cells. MEF vin- cells were stained with CMFDA and TaCT probe microscopy and flow cytometry analysis was performed ~1 hr after cell seeding. (B) Representative RICM, Cy3B, and Atto647N microscopy images of WT and vin- cells seeded on TaCT substrates separately. Intensity bar for Cy3B image indicates the % of TaCT probes that undergo force-triggered release while the intensity bar for Atto647N shows the signal normalized to the background. Scale bar = 10 μm. (C) Plots showed that tension signal (Cy3B, mean and integrated) and spreading area of WT cells were significantly higher than vin- cells (115 and 91 cells from n=3 replicates, geometric mean±95%CI, two-tailed student's t-test.) (D) Representative flow

cytometry density plot and quantification of force positive cells show that the WT cells had greater TaCT signal compared to vin- cells (n=4 replicates, mean±SEM, two-tailed paired student's t-test). (E) Schematic showing application of TaCT to co-cultured WT/vin- cells. (F) Representative RICM, Cy3B, and Atto647N microscopy images of co-cultured WT and vin- cells on TaCT substrate. Intensity bar for Cy3B image indicates the % of TaCT probes that undergo force-triggered release while the intensity bar for Atto647N shows the signal normalized to the background. Note that negative Atto647N signal for vin- cells was primarily due to cell-surface contact which alters the local index of refraction. (G) Representative flow cytometry density plot and quantification of force positive cells show that WT cells had significantly greater TaCT signal and force positive subpopulation compared to vin- cells incubated on the same TaCT substrate (n=4 replicates, mean±SEM, two-tailed paired student's t-test). (H) Schematic describes the TaCT experiments using MEF vin- cells transfected with different amounts of plasmid that encodes GFP-vinculin. (I) Plot shows the vinculin expression (x-axis, GFP MFI) versus TaCT signal (y-axis, Atto647N MFI) with different amounts of plasmid transfected (n=4 replicates). Green color represents the amount of the GFP-vinculin plasmid, the size of the bubble represents the % GFP positive subpopulation.